Colloids and Surfaces A: Physicochemical and Engineering Aspects 634 (2022) 128033

Contents lists available at ScienceDirect

Colloids and Surfaces A: Physicochemical and Engineering Aspects

journal homepage: www.elsevier.com/locate/colsurfa

Ambient-temperature porogen-free method for preparation of silica-based macroporous materials

Dan Trunov [a,*], František Muzika [b], Anita Kříž [a], Jiří Štětina [c], Ivona Sedlářová [d], Marcela Dendisová [e], Fatima Hassouna [f], Miroslav Šoóš [a,*]

[a] Department of Chemical Engineering, University of Chemistry and Technology, Technická 3, 166 28 Prague 6, Dejvice, Czech Republic
[b] Institute of Physical Chemistry Polish Academy of Sciences, Kasprzaka 44/52, 01-224 Warsaw, Poland
[c] Department of Dairy, Fat and Cosmetics, University of Chemistry and Technology, Technická 3, 166 28 Prague 6, Dejvice, Czech Republic
[d] Department of Inorganic Technology, University of Chemistry and Technology, Technická 5, 166 28 Prague 6, Dejvice, Czech Republic
[e] Department of Physical Chemistry, University of Chemistry and Technology, Technická 5, 166 28 Prague 6, Dejvice, Czech Republic
[f] Department of Computing and Control Engineering, University of Chemistry and Technology, Technická 5, 166 28 Prague 6, Dejvice, Czech Republic

GRAPHICAL ABSTRACT

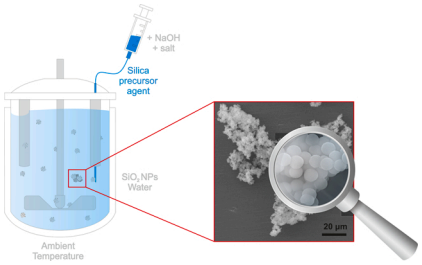

ARTICLE INFO

Keywords:
Macroporous material
Porogen-free method
Reactive gelation
Silica aggregation
Fractal aggregates
Enzyme immobilization

ABSTRACT

The presented work focuses on the synthesis of silica-based macroporous aggregates composed of silica nanoparticles using a template-free method. To improve the mechanical strength of the prepared fractal-like aggregates, the silica precursor tetraethyl orthosilicate (TEOS) is used during nanoparticle aggregation. The obtained results confirm the possibility to tailor the pore size distribution (PSD) simply by using primary particles of various sizes. The prepared porous materials have a porosity ranging from 60% to 74% with a specific surface area between 10 and 200 m^2/g and an average pore diameter from 30 to 1300 nm. Functionalization of the aggregate surface was done by replacing part of TEOS with a silica precursor that contained desired functional groups. This was demonstrated by preparing macroporous aggregates with carboxyl, amine and epoxy functional groups. The application of prepared aggregates was demonstrated by immobilization of urease from Canavalia ensiformis resulting in high enzyme activity compare to free enzymes.

* Corresponding authors.
E-mail addresses: dan.trunov@vscht.cz (D. Trunov), miroslav.soos@vscht.cz (M. Šoóš).

https://doi.org/10.1016/j.colsurfa.2021.128033
Received 5 October 2021; Received in revised form 27 November 2021; Accepted 29 November 2021
Available online 1 December 2021

1. Introduction

Silica is an important raw material used for a broad range of applications including chemistry [1], pharmaceuticals [2], insulation materials [3], separation or biosensing of various molecules [4,5], polishing, and dye manufacturing [6]. To prepare silica based macroporous materials, methods utilizing the sol-gel process combined with sacrificing templates, typically polymer nanoparticles, have been developed [7]. The major advantage of these methods is that due to the rather monodisperse distribution of polymeric nanoparticles, the formed pores also have a very narrow size distribution and thus can form an organized lattice morphology. Furthermore, depending on the used conditions, it is possible to prepare porous material in the form of individual hollow silica particles [8,9] with a solid core and a porous shell, or even monoliths [10]. Generality of this concept has also been demonstrated by use of other metal oxides apart from silica [11], which can be applied in catalysis or as a support in separation technologies. However, such templates have to be consequently removed by heat treatment of the prepared material, which often limits this method to production of supporting material [7]. Sometimes, further functionalization is required as separate step of material synthesis.

Another method that has been used to prepare macroporous silica materials with a spherical shape is spray drying. This method is based on the removal of the dispersing solvent, typically water, from the droplets containing silica nanoparticles. Due to the increase of solid content, silica nanoparticles start to fill the available space and form porous structures, with pores controlled by the size and concentration of the silica nanoparticles [12,13]. Furthermore, Chang et al. [12] demonstrated the possibility to modify the PSD of porous particles prepared by spray-drying using smaller silica aggregates compared to the suspension of stable silica nanoparticles. By the addition of templates, which could be either polymeric nanoparticles or dissolved polymer chains, followed by their calcination, Chang et al. were able to further modulate the pore structure of the formed particles [12]. Zellmer et al. [14] investigated the impact of various functional groups on the surface of silica nanoparticles during the spray-drying process. They found that the structure of the formed aggregates was almost independent of the type of functional groups attached to the surface of the silica particles, while there was a significant influence of the surface ligands on the mechanical properties of formed porous particles.

Methods based on various forms of emulsions as templates for macropores combined with the sol-gel process for preparation of macroporous particles or monoliths has been also used [15]. The emulsion-based method is often combined with the addition of polymer particles to produce hierarchical structures, where the polymer particles are then removed by calcination and thus provide additional porosity [16]. As discussed above, when a calcination step is required for the removal of the template, an additional step is needed to introduce surface functional groups.

Less frequent methods for preparation of macroporous materials employed spinodal decomposition [17], polymer induced aggregation [18] or ice templating [19]. In particular, Cademartiri et al. [18] used polyethylene glycol of various molecular weights, which was used as a guiling agent during the sol-gel process, leading to the formation of macroporous monoliths. Depending on the polyethylene glycol molecular weight, they were able to tune specific surface areas, ranging from tenths to hundreds of m^2/g, and average pore diameters, ranging from several nanometers up to tenths of nanometers. Galarneau et al. [17] have reported the preparation of macroporous material using a combination of polyethylene oxide and TEOS as the silica source. The obtained results, in the form of monoliths, have a large surface area of around 1300 m^2/g with an average pore diameter between 10 and 30 nm. However, this approach is not suitable for the production of porous materials with larger pores that are typically used for large biomolecule separation [20].

Zhao et al. [21] presented what the impact of temperature is during the porous material calcination step. They showed that by tailoring the calcination temperature, the porosity of the nanofoam can be controlled to around 60%, with an independent control for pore diameter.

The present work focuses on the preparation of macroporous microclusters using a method called reactive gelation. This method was initially developed for the production of polymeric macroporous material [22]. As has been recently shown [23–25], reactive gelation allows for the preparation of porous materials in the form of monoliths or microparticles with large pores, without using a template. In particular, polymeric nanoparticles are used as building blocks to construct fractal-like porous material. In addition, by varying processing conditions, it is possible to tune the broadness of the PSD [24–26]. Application of such material was demonstrated during separation of various molecules [20,27,28]. Building on this knowledge, the present study focuses on the preparation of macroporous microclusters, using silica nanoparticles as building blocks, with controllable porosity and PSD based on the aggregation process. Upon the destabilization of silica nanoparticles, addition of the silica precursor followed by the sol-gel process during nanoparticle aggregation was used to increase the strength of the formed clusters. Prepared aggregates were characterized by several analytical techniques to understand and describe the process of cluster formation. The obtained results confirm that the proposed approach is able to tailor the PSD of prepared materials without any template addition, simply by varying size of silica nanoparticles. In addition, we demonstrated that by using suitable silica precursors, we were able to prepare mechanically stable aggregates with various functional groups on their surface.

2. Materials and methods

2.1. Chemicals and reagents

Hydrochloric acid (35 wt%), high purity sodium hydroxide, ethanol for UV (99 wt%), ammonia solution (25 wt%), purity magnesium chloride hexahydrate (≥95 wt%), urea (≥99 wt% p.a.), tris(hydroxymethyl) aminomethane (≥99.8 wt%, TRIS) and dipotassium phosphate (99 wt% p.a.) were purchased from PENTA, Czech Republic. Ludox HS-40 colloidal silica 40 wt% suspension in water (lot 420816), high purity tetraethyl orthosilicate (≥99%, TEOS), high purity (3-Glycidyloxypropyl) trimethoxysilane (≥98%, GPTMS), high purity (3-Aminopropyl) triethoxysilane (≥99%, APTES), glutaraldehyde solution (25%, GA), urease from Canavalia ensiformis (15,000–50,000 units/g), Nessler's reagent for determination of ammonia and monopotassium phosphate (99 wt% p.a.) were obtained from Sigma-Aldrich. 3-(Triethoxysilyl) propyl succinic anhydride (60–70%, TESSA) was acquired from ABCR GmbH, Karlsruhe, Germany.

2.2. Synthesis of monodisperse SiO_2 nanoparticles

Synthesis of monodisperse silica nanoparticles with various diameters was done using a modified Stöber process [29–33]. In this work, nanoparticles with diameters ranging from 100 to 690 nm were prepared. The detailed amounts of reactants reaction temperatures, and times are shown in Table 1. Particles with a diameter of around 100 nm were prepared by mixing ethanol and ammonia (25 wt%) together and

Table 1
Conditions for preparation of silica nanoparticles with various sizes used in this work.

SiO_2 (nm)	EtOH (ml)	NH_3 (ml)	TEOS (ml)	Water (ml)	Time (h)	Temperature (°C)
100	900	67.5	27	0	24	60
180	68	1.9	6	25	24	25
260–400	40	10	20	35–40	12	80
690	57	9	30	34.62	12	80

heating the reaction in a three-neck round flask while stirring with a magnetic bar at 200 rpm. After 30 min, TEOS was rapidly added. 24 h later, the colloidal solution was cooled down to room temperature and was washed three times with ethanol and deionized water by centrifugation (10 min at 15,000 rpm).

The particles with 180 nm diameter were prepared in a two-neck round flask. First, ethanol, ammonia, and deionized water were stirred for 5 min using a magnetic stirrer operated at 300 rpm, followed by the fast addition of TEOS. The formed nanoparticles were washed three times with ethanol and deionized water by centrifugation (10 min at 10,000 rpm).

The synthesis of nanoparticles in the range 260–400 nm was performed in a round flask by mixing TEOS, ethanol, ammonia, and deionized water. After 30 min of homogenization using a magnetic stirrer operated at 300 rpm, the mixture was heated to the reaction temperature. The synthesized particles were washed three times with ethanol and deionized water by centrifugation (10 min at 8000 rpm).

For silica nanoparticles with a 690 nm diameter, TEOS was mixed with ethanol for a period of 15 min using a magnetic bar (250 rpm), followed by the addition of ammonia and deionized water. The obtained mixture was mixed for another 30 min before heating to the reaction temperature. Prepared particles were washed several times with ethanol and deionized water by centrifugation (10 min at 6000 rpm).

All synthesis materials were stored in water in a fridge for further use.

2.3. Aggregation of SiO_2 nanoparticles into porous clusters and their surface functionalization

Prior to the aggregation experiment, the critical coagulation condition (CCC) for each silica nanoparticle size was determined. This was done by visual observation of the local formation of large aggregates, which in the case of silica nanoparticles, settles down in the test vials. The experiment was carried out by adding a small amount of silica nanoparticles (typically 200 μL) into a 10 ml $MgCl_2$ solution of varying concentrations. Illustration of the results of this test is presented in Fig. SI 1 in Supporting Information [34].

Preparation of porous aggregates for all tested primary particle sizes was performed in the stirred reactor with a working volume of 150 ml. The reactor was filled with deionized water and the required amount of silica nanoparticle suspension such that the final concentration of silica nanoparticles was equal to 0.4 wt%. To minimize disturbance of the aggregation process, care was taken to remove air bubbles from the reactor. Then, sodium hydroxide was added into the reactor through an injection capillary to achieve pH 12, followed by 5 min of stirring using an overhead stirrer. Next, 3 M magnesium chloride solution was rapidly added to the reactor, resulting in its final concentration equal to 10 ×CCC. In this way, all primary particles were fully destabilized, resulting in their rapid aggregation [35]. After 10 min of mixing, an appropriate amount of a silica precursor (TEOS, APTES, GPTMS or TESSA) was added into the reactor to increase the mechanical strength of formed aggregates. Once the steady state size of aggregates was reached, the process was stopped by quenching the reaction mixture with 1000 ml of deionized water. To prevent long-term aggregation of the prepared clusters, deionized water was exchanged several times before the aggregates were stored in water for further analyses. The scheme of the process is shown in Fig. 1. As described above, the process contains several steps that can be done separately, thus providing flexibility to tune the final aggregate's properties. In the following, all process parameters which affect the final properties of macro-porous aggregates are discussed, i.e., stirring speed, amount and type of added silica precursor, time of silica precipitation during aggregation process and size of primary particles.

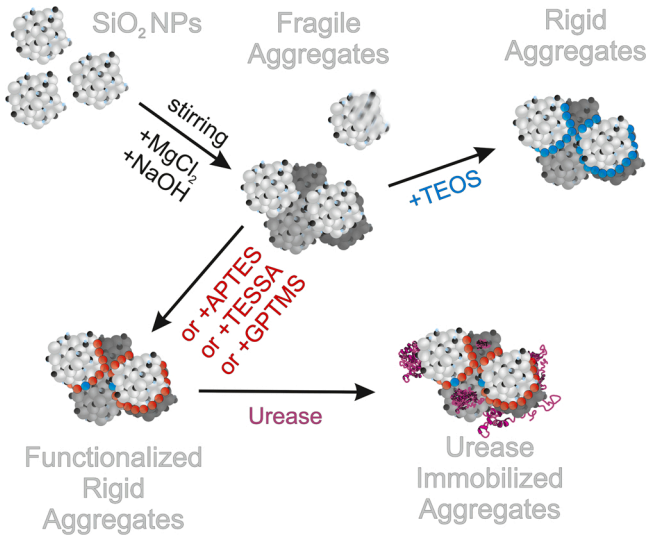

Fig. 1. Scheme diagram of the preparation and immobilized urease.

2.4. Immobilization of urease on aggregate

The immobilization process of urease was done using silica aggregates with several functionalized surfaces. First, silica aggregates containing amino groups (SiO_2-HN_2) were used as primary surface modified material [36]. Then, the modified material (2 mg) was suspended in phosphate-buffered saline (0.9 ml) and immersed in 10 vol% solution of GA for 3 h at ambient temperature. Modified aggregates containing GA groups (SiO_2-HN-GA) were washed several times with deionized water and dried in the oven overnight [37].

The dry materials SiO_2-HN-GA and SiO_2-HN_2 were then redispersed in a solution of phosphate-buffered saline while stirring, followed by a loading step using Jack bean urease (4 U/ml) solution. This was stirred for 1 h Then, the solution was placed under stagnant conditions in the fridge at 4 °C for 1 day, 3 days, 6 days and 10 days. Please note that 1 Unit corresponds to the amount of enzyme that catalyzes the conversion of 1 micro-mole of urea per minute (1 U = 1 μmol/min). The immobilized materials were filtered out by 0.45 μm PTFE filter and dried at ambient temperature.

2.5. Characterization techniques

2.5.1. Dynamic light scattering

The size of the primary particles was determined by dynamic light scattering using Zetasizer Nano (Malvern, UK). The measurements were set to automatic mode at ambient temperature and a fixed scattering angle of 173°. All measurements were performed at least three times and the average particle size was extracted from an autocorrelation function.

2.5.2. Static light scattering (SLS)

The size of clusters and their fractal dimensions were analyzed by static light scattering using Mastersizer 2000 (Malvern, UK). Testing of the mechanical stability of aggregates prepared with and without TEOS was done in a dispersion unit Hydro 2000 G (Malvern, UK) connected to Mastersizer 2000. Prepared aggregates were characterized by mean radius of gyration ($\langle R_g \rangle$), which was evaluated from the measured light scattering data using the Guiner approximation of structure factor $S(q)$ [38], defined as:

$$S(q) = \frac{I(q)}{I(0)\,P(q)} \cong \exp\left(-\frac{q^2}{3} \left\langle R_g^2 \right\rangle_{S(q)} \right) \quad (1)$$

Here, $I(0)$ is the zero angle intensity, $P(q)$ is the form factor (due to primary particles) and $I(q)$ is the angle dependent intensity of scattered light. The scattering vector amplitude, q, is defined as:

$$q = 4\pi\frac{n}{\lambda}\sin(\theta/2) \tag{2}$$

and contains information about the detector positions in terms of the scattering angle, θ, refractive index of the dispersing fluid, n, and the laser wavelength in vacuum, λ.

The $\langle R_g^2\rangle_{S(q)}$ in Eq. (1) determined from the slope of the linear relationship between $\ln(I(q)/P(q))$ and $q^2/3$ [39,40], was consequently used to evaluate the mean radius of gyration of the aggregate population: $\langle R_g^2\rangle = \langle R_g^2\rangle_{S(q)} + \langle R_{g,p}^2\rangle$. The $\langle R_{g,p}\rangle$ corresponds to the radius of gyration of primary particles, which can be easily calculated from their measured hydrodynamic radius [41].

Another parameter which can be estimated from the light scattering data, in particular from the slope of the power law region of the log-log plot of $S(q)$ vs. q, is the aggregate fractal dimension, d_f. However, as it was shown by Ehrl et al. [42] or Lattuada et al. [43] this approach is applicable only for primary particles with diameters substantially smaller than the wavelength of the laser. For larger particles, the slope of log-log plot of $S(q)$ vs. q deviates from the aggregate fractal dimension and another technique has to be used.

2.5.3. Optical microscopy

In particular, d_f of aggregates composed of primary particles comparable to or larger than the laser wavelength can be estimated from 2D aggregate images. In this work, images were obtained using Nikon ECLIPSE LV 150 N (Nikon, JP), followed by plotting the projected surface area occupied by an aggregate as a function of its perimeter. By extracting the power-law of $A \propto P^{2/d_{pf}}$, it is possible to obtain the perimeter fractal dimension d_{pf}. Consequently, this can be converted to mass fractal dimension using the correlation derived by Ehrl et al. [44], of the form:

$$d_f = -1.5 * d_{pf} + 4.4 \tag{3}$$

2.5.4. Scanning electron microscopy (SEM)

The morphology of the prepared aggregates was further characterized by a scanning electron microscope, VEGA3 SBU (Tescan, CZ) operated at 30 kV, using a detector of secondary electrons. The sample of macroporous aggregates were diluted with deionized water and dried overnight on the SEM target at ambient temperature, followed by applying gold sputter coating with a thickness of 10 nm.

2.5.5. Nitrogen sorption and mercury porosimetry

The specific surface area for all dried samples was obtained from the Brunauer-Emmelt-Teller equation [45] using the nitrogen sorption device Quantachrome Nova 2200e (Anton-paar, AUT). Samples were degassed under vacuum at 250 °C at least 48 h before measurement. Further analysis of large pores and aggregate porosity was done by intrusion mercury porosimetry using a Micromeritics Autopore IV 9500 (Microtrac, DE). Prior to analysis, the samples were oven-dried overnight at 80 °C.

2.5.6. Fourier transform infrared spectroscopy (FTIR)

To confirm presence of various functional groups on the surface of prepared porous material, FTIR analysis was performed. Powder containing KBr and a small amount of dry material was manually compressed using a tableting machine. FTIR in transmission mode was performed on the prepared pellets using a Nicolet FTIR spectrometer Nexus 670 (Thermo Scientific, USA) with 128 scans and a resolution of 4 cm^{-1}. Measurements were analyzed with OMNIC Software.

2.5.7. Colloidal titration

Backward colloidal titration was used to determine the amount of groups on the surface while measuring the conductivity of the remaining solution (this was done only for aggregates containing amino or carboxylic surface groups). In particular, for colloidal titration, 1 ml of aggregates composed of silica nanoparticles modified with APTES (TESSA) was dispersed in 150 ml of deionized water. Then, an excessive amount of hydrochloric acid (sodium hydroxide) 10 mM was added to completely neutralize the amine (carboxylic) surface groups. Excess of hydrochloric acid (sodium hydroxide) was consequently determined by titration with 10 mM sodium hydroxide (hydrochloric acid) at constant stirring [46].

2.5.8. Determination of unreacted amount of TEOS

The measurement of unreacted TEOS after aggregation process was done by the decantation method using a separating funnel. Since TEOS and water are immiscible liquids, a small layer of unreacted TEOS was created on the top of the water phase. After careful removal of the water phase, the volume of unreacted TEOS was determined. To minimize the experimental error, the measurement was performed at least three times, and the presented values represent the average values with their corresponding standard deviation.

2.5.9. Determination of the amount of immobilized urease

The amount of released ammonia from immobilized urea was determined spectrophotometrically at 480 nm in a UV-Vis spectrophotometer, Agilent 8454 (Agilent, USA). The intensity of the colored ammonia compound formed after the addition of Nessler's reagent was measured. Activity of free urease solution was measured in the same way and used as a comparison to evaluate the activity of the enzyme immobilized on the porous silica aggregates.

2.5.10. Fluid flow characterization

To obtain a quantitative relationship between the size of macroporous aggregates and the hydrodynamic conditions applied during their synthesis [47], the fluid flow inside the stirred reactor was characterized by Computational Fluid Dynamics simulations using the commercial software ANSYS Fluent v19.2. To obtain mesh independent solutions for stirring speeds from 50 to 800 rpm, the computational grid used to discretize the stirred vessel contained approximately 1.6×10^6 elements. Due to the absence of baffles in the bottom part of the vessel, turbulence was modeled by a realizable k-ε model [48], while flow near the wall was modeled by applying a standard wall function [49]. Due to the low solid volume fraction (0.4 wt%), the flow field was simulated using a single phase model with a density and viscosity of water at 20 °C, i.e. equal to 1000 kg/m^3 and 1 mPa.s, respectively. The average energy dissipation rate in the system was calculated from the ratio of the power input, P, over the liquid mass, m, according to:

$$\langle\varepsilon\rangle = \frac{P}{m} = \frac{\omega\int_A \mathbf{r}\times(\tau\cdot d\mathbf{A})}{m} \tag{4}$$

(Table 2) Here, A is the surface of impeller and shaft, ω is the angular velocity vector (in rps), r is the position vector, τ is the stress tensor, and $d\mathbf{A}$ is the differential surface vector. The obtained values of $\langle\varepsilon\rangle$ were used to evaluate the average shear rate$\langle G\rangle$ according to:

Table 2
Hydrodynamic conditions used in stirred tank during synthesis of silica aggregates.

Stirring speed (rpm)	Impeller *Re* (-)	$\langle\varepsilon\rangle$ (m2/s3)	$\langle G\rangle$ (1/s)
50	2083	2.26×10^{-3}	39.5
100	4167	1.58×10^{-2}	99.6
200	8333	0.111	250.0
400	16,667	0.786	638.1
800	33,333	5.63	1672.7

$$\langle G \rangle = \sqrt{\frac{\langle \varepsilon \rangle \rho}{\mu}} \quad (5)$$

3. Results and discussion

3.1. Impact of silica precursor on the strength of prepared aggregates

The presented method uses silica primary particles as building blocks for preparation of macroporous aggregates. A scheme of the whole procedure, including the locking step to improve the mechanical strength of the formed aggregates, their functionalization, and their immobilization is presented in Fig. 1. Upon their destabilization and consequent aggregation, typical silica nanoparticles form fractal-like aggregates [50], where the primary particles are held together by the action of van der Waals forces. Since such aggregates are very fragile, a locking step was introduced, resulting in the formation of new silica layer on the surface of primary particles, causing their interconnection. In this way, the strength of interparticle connections increases substantially, as is demonstrated in Fig. 2, which shows a comparison of the aggregate's mean radius of gyration, $\langle R_g \rangle$, measured for two different cluster types composed of the same silica nanoparticles. As can be seen in Fig. 2, aggregates formed without the addition of TEOS precursor, i.e. where primary particles were held together only by the van der Waals force (open symbols), have significantly smaller $\langle R_g \rangle$ compare to those prepared in the presence of TEOS precursor (solid symbols) when exposed to increasing stirring speed in the dispersion unit. Data presented for zero stirring speed correspond to the aggregates prepared in the stirred reactor, which were gently withdrawn, diluted with deionized water, and injected into the measuring cell of Mastersizer 2000 by syringe. It is worth noting that several tests were performed to evaluate the impact of sample withdrawal and manipulation on possible variation of the particle size [47,51].

Based on these results, a systematic study of the impact of silica precursor amount on the size of formed aggregates was carried out. In Fig. 3a shows a summary of these experiments, indicating that there exists a certain minimum amount of silica precursor for which there is observed significant increase of the aggregate strength. In particular, for the studied primary particles with 25 nm diameter this is about 0.1 ml of TEOS, which was added into a 150 ml reactor and corresponds to 0.067 vol%. When considering the total surface area of all primary particles, with the assumption that the new silica layer would coat every particle homogeneously, the result would be a layer thickness of about 0.7 nm. In fact, as can be seen in Fig. 3b, there is an observed correlation of individual primary particles supporting the growth of a new silica layer on the surface of every particle during production of porous material. Since the aggregation process is also combined with the break-up of newly formed aggregates, another parameter to be considered is the time of the process when aggregate strength becomes lower than the applied stress [52–55]. Fig. 4 presents time evolution of $\langle R_g \rangle$ measured for four different primary particle sizes: 25, 100, 400 and 690 nm, respectively. It can be seen that for all tested primary particle sizes, the steady state is reached approximately after 100–200 min (see Fig. 4a). This is further supported by the measurement of TEOS conversion, which is shown in Fig. 4b. In fact, reaching steady state size is well correlated with complete consumption of TEOS, which reaches 0 mol/L after around 200 min, with the exception of smaller primary particles, where the complete conversion is reached a bit earlier. Based on these results, all further experiments were performed with 6 ml of the silica precursor, and aggregate preparation was carried out over the period of 240 min

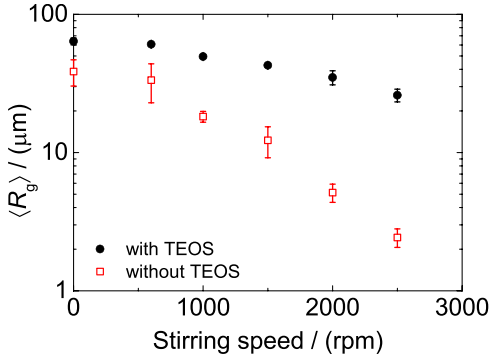

Fig. 2. Radius of gyration of the aggregates composed of silica nanoparticles with diameter 25 nm measured for various stirring speed in dispersion unit Hydro 2000 G.

In addition, for the primary particles with 260 nm diameter, the process of aggregate formation in the presence of 6 ml of silica precursor (TEOS) was investigated. Fig. 5a–d presents SEM images measured in time intervals of 15 min, 30 min, 1 h and 2 h. As can be seen, ordering particles to the final shape of aggregate starts within in 15 min (see Fig. 5a). The formation of the second layer and connection of individual particles with the silica precursor is visible after 30 min during the aggregation process (see Fig. 5b). As the time proceeds, silica nanoparticles continue to become more and more interlocked, leading to the final aggregate pore structure (see Fig. 5c and d). In fact, as observed in Fig. 5d, there is a small layer of new silica with thickness from about 10 nm up to 50 nm formed between individual nanoparticles.

3.2. Morphology of prepared aggregates and scaling of aggregates size with applied shear rate

SEM images of the prepared aggregates using a broad range of primary particles are presented in Fig. 6. As can be seen in all cases, aggregates have a fractal structure with well-preserved primary particles. Furthermore, due to their nature, these aggregates also contain many pores which are present in the empty space in between interconnected primary particles.

To quantify the compactness of the prepared aggregates, their internal structure was characterized by fractal dimension. It was shown by several authors that for compact aggregates prepared under fully destabilized conditions in the presence of shear, typical values of d_f are in the range from 2.6 to 2.9 [24–26,42,51,56,57]. In contrast, values of d_f for more open aggregates, prepared under stagnant conditions, vary in the range from 1.8 to 2.1 depending on the degree of primary particle destabilization. Lower values are typical for fully destabilized particles, i.e., Diffusion-Limited Colloid Aggregation [35], while higher values around 2.1 are typical for partially destabilized particles aggregated under the action of Brownian motion [58].

Since primary particles with diameters in the range of 25–690 nm were used in this work, a combination of techniques to estimate d_f was employed. In particular, for small particles, where the size is in the limit of Rayleigh-Debye-Gans theory [59,60], it is possible to estimate d_f from the slope of the log-log plot $S(q)$ vs. q. Examples of such plots obtained for primary particles with diameters 25 nm and 100 nm, respectively, are presented in Fig. 7a and b. As can be seen, both datasets obtained for four different stirring speeds can be well approximated by the same power-law curve with a slope equal to 2.7. For larger primary particles, another approach based on the evaluation of perimeter fractal dimension d_{pf} [42,57] was used. In particular, d_f equal to 2.6 was estimated from the correlation between d_f and d_{pf} developed by Ehrl et al. [44] confirmed the compact structure of the prepared aggregates.

Another characteristic of the studied system, which can be validated against considered theoretical models, is the scaling of the steady state aggregates $\langle R_g \rangle$ as a function of applied shear rate. Obtained scaling for three different particle sizes: 25, 100 and 400 nm, is presented in Fig. 8. As can be seen, all measured data can be well approximated by a power-law scaling using the same exponent equal to −0.52. This value agrees

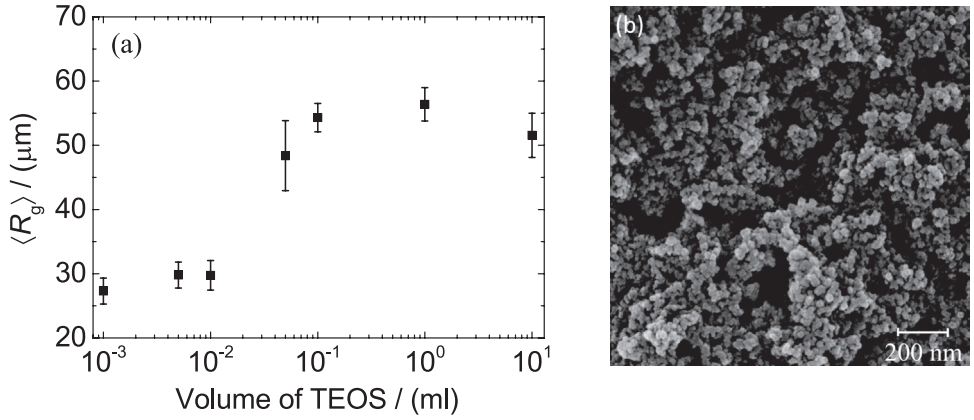

Fig. 3. (a) Radius of gyration of the clusters vs. concentration of TEOS in reactor for primary nanoparticles of size 25 nm. (b) SEM image of the surface of porous aggregates prepared from 25 nm silica primary particles indicating interconnection of particles.

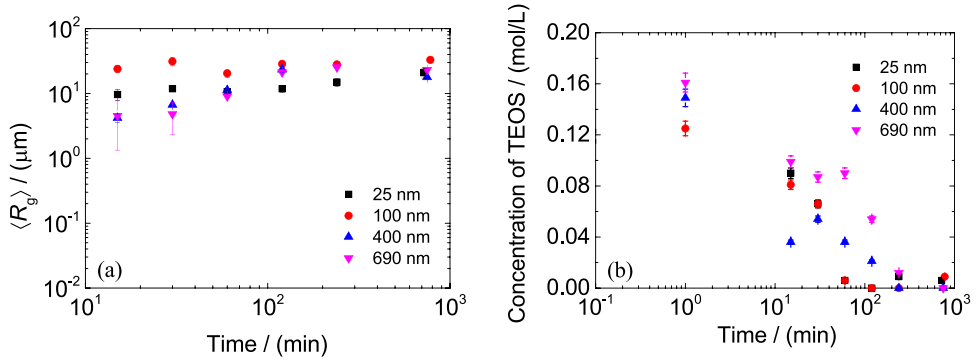

Fig. 4. (a) Trend of the aggregates size evolution as a function of aggregation time for different primary particle sizes. (b) Time evolution of the kinetics of the TEOS concentration as a function of aggregation time for different particle sizes.

very well with the theoretically predicted scaling of steady state aggregate sizes as a function of applied shear rate developed by Zaccone et al. [52], where d_f equal to 2.7 was determined experimentally using SLS or image analysis (see Fig. 7).

3.3. Effect of nanoparticles size on the porous structure of aggregates

To characterize PSD, porosity and specific surface area of the prepared porous aggregates and their detailed characterization was performed using a combination of several analytical techniques. Fig. 9 summarizes all measured quantities. As can be seen in Fig. 9a, the amount of adsorbed N_2 is inversely dependent on the size of silica nanoparticles, with the highest values of almost 100 cm^3/g correlated with the smallest particles. In contrast, as the primary particle size decreased by one order of magnitude, the amount of adsorbed nitrogen decreased by almost two orders of magnitude, clearly indicating a substantial change of the size of the pores and their structure. This is further confirmed by the measuring of Hg intrusion porosimetry shown in Fig. 9b. As can be seen, the highest intruded volume was measured for porous aggregates prepared from silica nanoparticles with a diameter equal to 180 nm. In the case of 400 nm particles, intruded volume slightly decreased, while substantially lower values were measured for the smallest primary particles. In addition, as the primary particle diameter decreased, a shift was observed of the onset of Hg intruded volume towards higher pressures. This clearly indicates the presence of smaller pores, as previously observed by N_2 sorption measurement. Comparison of the PSD of prepared aggregates is presented in Fig. 9c. As can be seen in all cases, the PSD is characterized by a rather sharp peak and is controlled by the primary particle size. Considering the precise control of primary particle size during aggregate synthesis, this represents a significant advantage for preparation of porous material with tailored PSD without the necessity of using a sacrificing template. Shift of the mean pore size to smaller values with decreasing primary particle size is also connected to the significant increase of the specific surface area, from approximately 10 m^2/g measured for 400 nm primary particles, up to 200 m^2/g measured for 25 nm primary particles. In addition, this change is also connected to the increase of porosity from 60% up to 74% (see Fig. 9d). When comparing these results with those measured for porous materials prepared from polymeric primary particles of comparable sizes [20,23–26], we found good agreement supporting the generality of the proposed method of reactive gelation.

3.4. Surface modification during aggregation process

Since one of the potential application areas of porous materials is enzyme immobilization, we focused on the functionalization of the pore surface by various surface groups in this part. A significant advantage of the proposed method is that the functionalization with desired surface groups can be done easily during the preparation of porous aggregates, simply by replacing part of TEOS precursor with a suitable silica-based precursor. Here we demonstrate this by surface functionalization of the porous aggregates by introducing various functional groups: amino, epoxy and carboxyl groups. A summary of the analysis of these functional groups is presented in Fig. 10. In particular, Fig. 10a shows FTIR spectra of the porous aggregates functionalized with carboxyl and epoxy groups. As can be seen, all samples exhibited two common absorption bands at 1100 and 3400 cm^{-1} corresponding to Si-O asymmetric stretching of Si-O-Si groups and -OH stretching typical for the silanol functions (Si–OH), respectively. Moreover, the broad feature centered at 3400 and weak absorption band at 1638 cm^{-1} indicate that some water

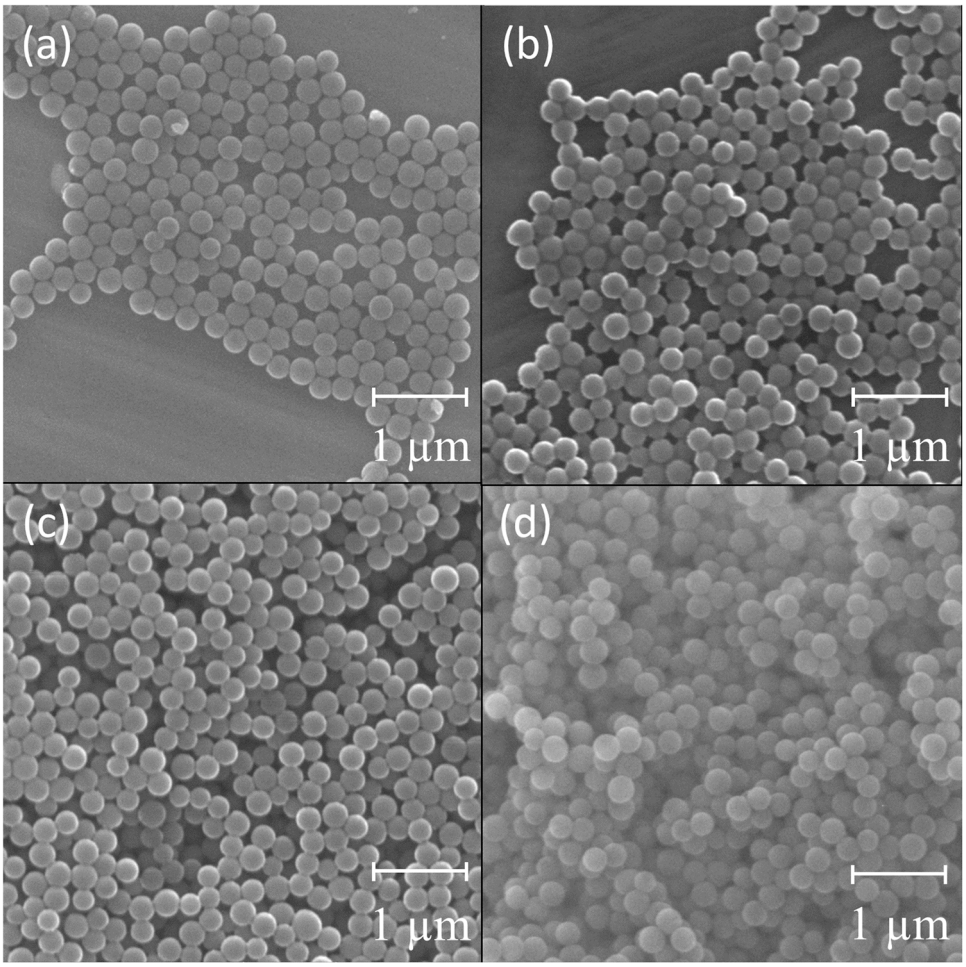

Fig. 5. SEM images of the individual particles prepared from 260 nm silica primary particles with fixed amount of TEOS at different time interval (a) 15 min; (b) 30 min; (c) 1 h; (d) 2 h.

is adsorbed at the surface of silica particles. Unlike in porous aggregates prepared by pure TEOS, additional peaks can be observed in GPTMS and TESSA based porous aggregates. Indeed, FTIR spectra of GPTMS porous aggregates exhibits absorption bands at 2860 cm^{-1} and 910 cm^{-1}, corresponding to $–CH_2$ and -CH stretching vibrations of alkyl groups and epoxy ring vibrations, respectively [61]. In TESSA based porous aggregates, appearance of the absorption band at 1700 cm^{-1} corresponding to C═O stretching vibrations typical for carboxylic acid groups confirm the hydrolysis of anhydride functions in water, leading to the formation of carboxylic acids. Due to the difficulty of detecting aliphatic amines by FTIR, titration (Fig. 10b) and Energy-dispersive X-ray spectroscopy (SI Fig. 2c) methods were used to detect amine groups in APTES based porous aggregates. Both methods detected a small amount of amino groups or nitrogen present on the surface of the aggregates. In addition, during Energy-dispersive X-ray analysis of aggregates coated with GPTMS and TESSA precursors, an increasing trend corresponding to peaks of carbon or oxygen elements was detected, confirming deposition of the precursor on the surface of the porous material.

Determination of the quantity of amino and carboxylic groups on the surface of the aggregates was done by backward colloidal titration, which was introduced earlier. Fig. 10b represents the number of groups depending on the volume of added precursor TESSA or APTES. As can be seen in both cases, an exponential dependence on the amount of added precursor is observed. However, the quantity of amino groups is much lower compared to TESSA due to the reactivity of APTES with oxygen in atmosphere. Based on these results, the quantity of the functional groups is strictly controlled by the concentration of the used precursor. Since surface modification of the porous aggregates can be easily done by replacement of the used precursors, the various combination of TEOS, TESSA, APTES, GPTMS, and others can increase potential usage of the material. However, type of the precursors can significantly affect the surface properties of the prepared material. In this case, of APTES and TESSA obtained specific surface area was equal to 57.9 and 55.4 m^2/g, respectively, which is comparable with the specific surface area of TEOS (60.8 m^2/g). In contrast, when GPTMS precursor was used for surface functionalization surface area was below the detection limit of the device. The similar trend was observed also in the case of porosity, where TEOS, APTES and TESSA have range from 63% to 70%, while for GPTMS porosity was 3 times smaller and equal to 20%. Such kind of difference in the porosity reflects the affinity of the surface groups to the water environment.

3.5. *Activity of immobilized urease on the modified surfaces*

In the last part of our investigation, we focused on the possible application of prepared aggregates for enzyme immobilization. Urease extracted from the Canavalia ensiformis, belonging to the superfamily of amidohydrolases and phosphotriesterases, was chosen as the test system for covalent bonding on the surface of SiO_2-HN-GA and SiO_2-HN_2 functionalized material. Stability of the enzyme bounded to functionalized surfaces is summarized in Fig. 11. Repetition of the urea hydrolysis was performed by reusing immobilized material. As can be seen in

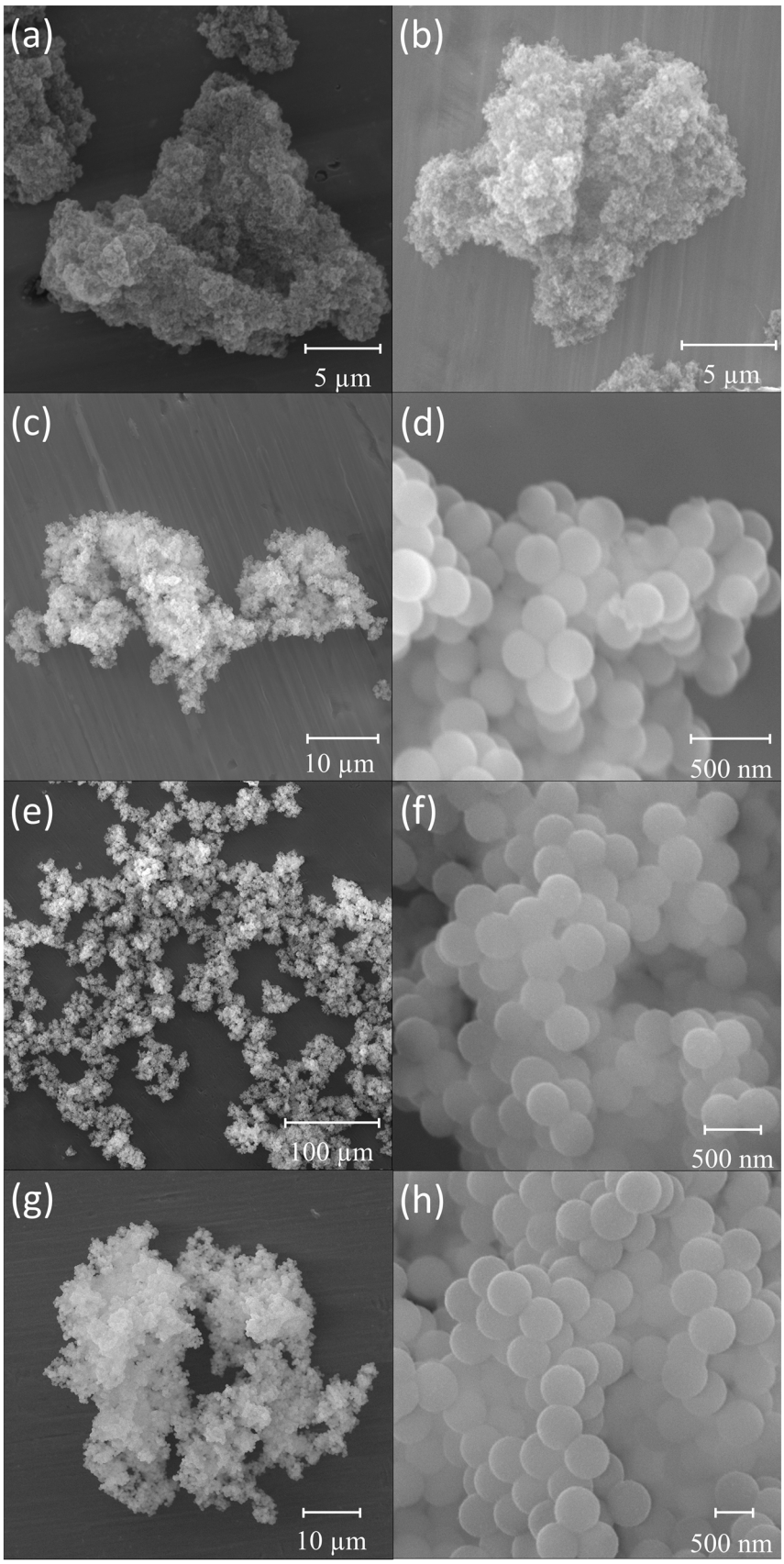

Fig. 6. SEM images of the prepared clusters with constant amount of TEOS and with constant time during aggregation using primary particles with sizes: (a) 25 nm; (b) 100 nm; (c, d) 260 nm; (e, f) 400 nm; (g, h) 690 nm.

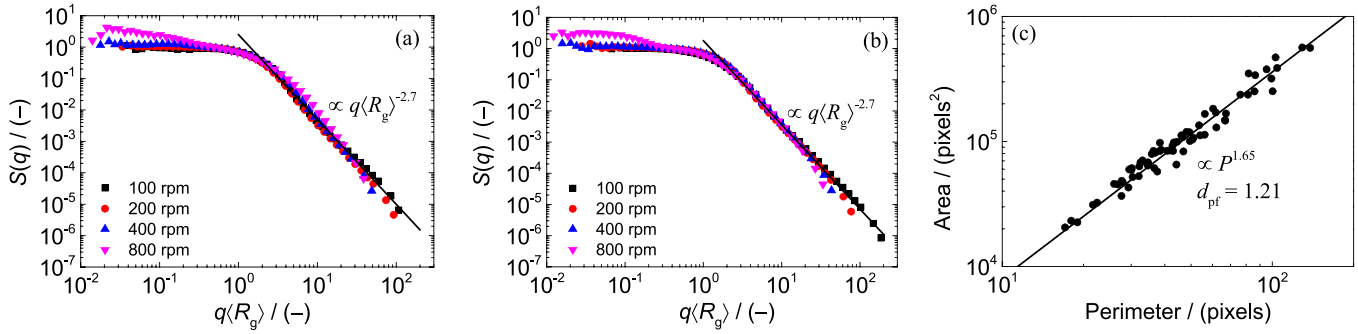

Fig. 7. Log-log plot of $S(q)$ and $q\langle R_g\rangle$ for determination of the fractal dimension of primary particles with diameters 25 nm (a) and 100 nm (b). Panel (c) presents scaling of the projected area of aggregates as a function of their perimeter used to determine the perimeter fractal dimensions for silica nanoparticles with a diameter of 400 nm.

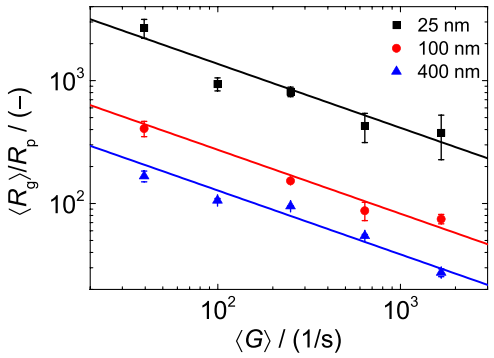

Fig. 8. Scaling of normalized steady state $\langle R_g\rangle/R_p$ as a function of the mean shear rate $\langle G\rangle$. The lines represents the theoretical scaling calculated according to Zaccone et al.[52] using d_f determined from light scattering data presented in Fig. 7.

Fig. 11a, when using free urease the process is irreversible, strongly decreasing the free enzyme activity only after one usage. In the case of functionalized material containing only amino groups, the enzyme activity was preserved after a second repetition, while a sharp decrease of enzyme activity (lower than 10% of original value) was observed for during the third repetition. The immobilized urease on the SiO_2-HN-GA aggregates was stable for three consecutive repetitions and retained 87% of the residual activity. This observation is comparable to the one reported by Chaudhari et al. [62] where activity of immobilized urease was found at 89% after third repetitions.

Finally, the long-term stability of immobilized enzyme on the surface of the macroporous aggregates, under ambient laboratory temperature of 23 ± 1°, is shown in Fig. 11b. While the activity of free urease is 85% after 2 days and 62% after 9 days, immobilized urease on the surface of SiO_2-HN_2 has the same activity of 85% after 2 days and 9 days. In the case of the modified material SiO_2-HN-GA, its activity is enhanced to 114% and decreases to 99% after 9 days.

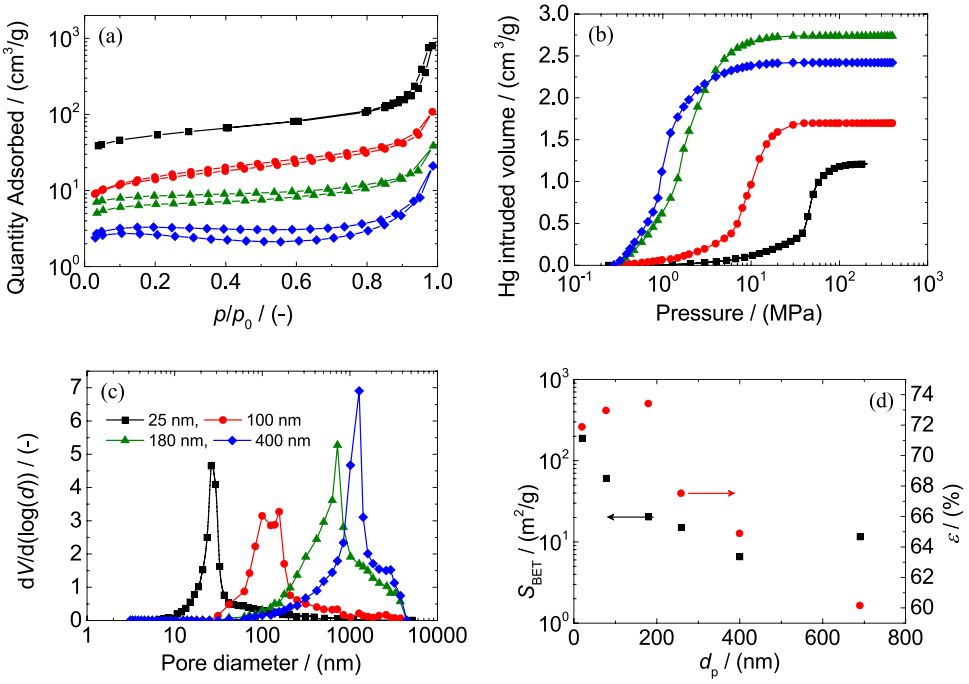

Fig. 9. (a) Nitrogen physisorption curves measured for aggregates composed of various sizes of primary particles together with intrusion curves obtained by mercury porosimetry (b). Panel (c) presents PSD recalculated from the intrusion curves. Panel (d) presents summary of the measured surface area and porosity for the prepared aggregates as a function of the primary particle size.

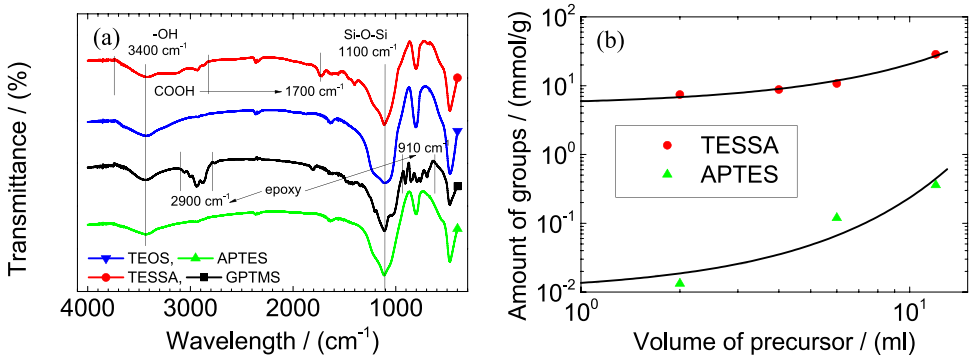

Fig. 10. (a) FTIR spectra of the material using different type of precursors for surface modification of the clusters. (b) Determination of the amount of surface groups using potentiometric titration of colloidal solution.

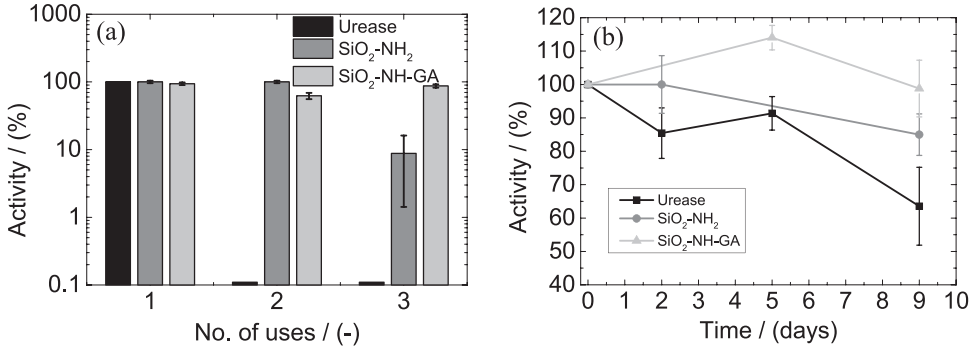

Fig. 11. (a) Repetition of the enzymatic reaction of the immobilized urease (4 U/ml) using 0.123 M urea, under pH= 7.0 (Tris buffer) and 30 °C. (b) Activity of immobilized urease during storage time at laboratory temperature 23 ± 1 °C using 0.123 M urea under pH = 7.0 (Tris buffer).

4. Conclusions

In this work, we presented a template-free procedure for the synthesis of macroporous aggregates composed of silica nanoparticles used as building blocks. Using this approach, we were able to prepare porous aggregates of compact structure and round shape, as confirmed by light scattering and image analysis. After detailed analysis of the used precursor, it was found that the strength of the formed aggregates is due to growth of the surface layer of silica on particles, resulting in their interlocking. Furthermore, by changing the size of silica nanoparticles, we were able to tune the porosity to be in the range of 60–74%, and PSD of the prepared aggregates to be in the range of 30–1300 nm. The proposed method is also suitable for the direct functionalization of the porous material surface by simply adding silica precursors containing desired functional groups during the particle assembly step. The immobilized urease from Jack bean was stable at ambient temperature for at least 9 days, and the reusability was examined for 3 cycles without significant loss in activity. Since the synthesis is done in a liquid phase, the presented method does not require any calcination to remove template particles, and thus produced macroporous aggregates that can be directly used in applications, including biocatalysis or separation of various molecules.

CRediT authorship contribution statement

Dan Trunov: Conceptualization, Methodology, Validation, Formal analysis, Investigation, Writing – original draft, Visualization. **František Muzika:** Methodology, Formal analysis, Investigation, Resources, Writing – review & editing, Funding acquisition. **Anita Kříž:** Validation, Writing – review & editing, Visualization. **Jiří Štětina:** Formal analysis, Resources. **Ivona Sedlářová:** Validation, Formal analysis. **Marcela Dendisová:** Validation, Formal analysis, Writing – review & editing. **Fatima Hassouna:** Formal analysis. **Miroslav Šoóš:** Conceptualization, Resources, Writing – review & editing, Visualization, Supervision, Funding acquisition.

Declaration of Competing Interest

The authors declare that they have no known competing financial interests or personal relationships that could have appeared to influence the work reported in this paper.

Acknowledgements

This work was supported by a Czech Science Foundation (GACR) grant 16-22997S and a Specific University Research – grant No A1_FCHI_2021_005.

This publication is part of a project that has received funding from the European Union's Horizon 2020 research and innovation program under the Marie Skłodowska-Curie Grant agreement No. 847413.

Scientific work published as part of an international co-financed project founded from the program of the Minister of Science and Higher Education entitled "PMW" in the years 2020 - 2024; agreement no. 5005/H2020-MSCA-COFUND/2019/2.

Appendix A. Supporting information

Supplementary data associated with this article can be found in the online version at doi:10.1016/j.colsurfa.2021.128033.

References

[1] V. Meynen, P. Cool, E.F. Vansant, Verified syntheses of mesoporous materials, Microporous Mesoporous Mater. 125 (2009) 170–223.

[2] X. Chen, Core/shell structured silica spheres with controllable thickness of mesoporous shell and its adsorption, drug storage and release properties, Colloids Surf. A Physicochem. Eng. Asp. 428 (2013) 79–85.
[3] Y.-S. Cho, D. Lee, Synthesis of macroporous silica particles by continuous generation of droplets for insulating materials, J. Nanosci. Nanotechnol. 18 (2018) 6112–6121.
[4] N.K. Bebris, A.V. Kiselev, B.Y. Mokeev, Y.S. Nikitin, Y.I. Yashin, G.E. Zaizeva, Macroporous silica as an adsorbent for molecular chromatography, Chromatographia 4 (1971) 93–97.
[5] K. Min, W. Choi, M. Choi, Macroporous silica with thick framework for steam-stable and high-performance poly(ethyleneimine)/silica CO_2 adsorbent, ChemSusChem 10 (2017) 2518–2526.
[6] Y. Chen, Y. Wang, J. Qin, A. Chen, Core/shell structured solid-silica/mesoporous-silica microspheres as novel abrasives for chemical mechanical polishing, Tribol. Lett. 58 (2015) 37.
[7] Y. Bao, C. Shi, T. Wang, X. Li, J. Ma, Recent progress in hollow silica: template synthesis, morphologies and applications, Microporous Mesoporous Mater. 227 (2016) 121–136.
[8] C. Ge, D. Zhang, A. Wang, H. Yin, M. Ren, Y. Liu, T. Jiang, L. Yu, Synthesis of porous hollow silica spheres using polystyrene–methyl acrylic acid latex template at different temperatures, J. Phys. Chem. Solids 70 (2009) 1432–1437.
[9] Z. Teng, Y. Han, J. Li, F. Yan, W. Yang, Preparation of hollow mesoporous silica spheres by a sol–gel/emulsion approach, Microporous Mesoporous Mater. 127 (2010) 67–72.
[10] Y. Hotta, P.C. Alberius, L. Bergström, Coated polystyrene particles as templates for ordered macroporous silica structures with controlled wall thickness, J. Mater. Chem. 13 (2003) 496–501.
[11] B.T. Holland, C.F. Blanford, T. Do, A. Stein, Synthesis of highly ordered, three-dimensional, macroporous structures of amorphous or crystalline inorganic oxides, phosphates, and hybrid composites, Chem. Mater. 11 (1999) 795–805.
[12] H. Chang, H.D. Jang, Controlled synthesis of porous particles via aerosol processing and their applications, Adv. Powder Technol. 25 (2014) 32–42.
[13] H. Lv, F. Meng, M. Zhang, Z. Geng, Y. Sun, Effect of the drying process on the preparation of porous silica microspheres, Chem. Eng. Sci. 135 (2015) 285–293.
[14] S. Zellmer, M. Lindenau, S. Michel, G. Garnweitner, C. Schilde, Influence of surface modification on structure formation and micromechanical properties of spray-dried silica aggregates, J. Colloid Interface Sci. 464 (2016) 183–190.
[15] M. Fujiwara, K. Shiokawa, I. Sakakura, Y. Nakahara, Preparation of hierarchical architectures of silica particles with hollow structure and nanoparticle shells: a material for the high reflectivity of UV and visible light, Langmuir 26 (2010) 6561–6567.
[16] Y.-S. Cho, G.-R. Yi, S.-H. Kim, D.J. Pine, S.-M. Yang, Colloidal clusters of microspheres from water-in-oil emulsions, Chem. Mater. 17 (2005) 5006–5013.
[17] A. Galarneau, Z. Abid, B. Said, Y. Didi, K. Szymanska, A. Jarzębski, F. Tancret, H. Hamaizi, A. Bengueddach, F. Di Renzo, F. Fajula, Synthesis and textural characterization of mesoporous and meso-/macroporous silica monoliths obtained by spinodal decomposition, Inorganics 4 (2016) 9.
[18] R. Cademartiri, M.A. Brook, R. Pelton, J.D. Brennan, Macroporous silica using a "Sticky" Stöber process, J. Mater. Chem. 19 (2009) 1583–1592.
[19] H. Nishihara, S.R. Mukai, D. Yamashita, H. Tamon, Ordered macroporous silica by ice templating, Chem. Mater. 17 (2005) 683–689.
[20] B.C. de Neuville, A. Lamprou, M. Morbidelli, M. Soos, Perfusive ion-exchange chromatographic materials with high capacity, J. Chromatogr. A 1374 (2014) 180–188.
[21] C. Zhao, M. Wang, Y. Shi, J. Cao, Y. Qiao, High-temperature post-processing treatment of silica nanofoams of controlled pore sizes and porosities, Mater. Des. 90 (2016) 815–819.
[22] M.S. Silverstein, Emulsion-templated porous polymers: a retrospective perspective, Polymer 55 (2014) 304–320.
[23] N. Marti, F. Quattrini, A. Butté, M. Morbidelli, Production of polymeric materials with controlled pore structure: the "Reactive Gelation" process, Macromol. Mater. Eng. 290 (2005) 221–229.
[24] A. Lamprou, I. Köse, Z. Peña Aguirre, G. Storti, M. Morbidelli, M. Soos, Macroporous polymer particles via reactive gelation under shear: effect of primary particle properties and operating parameters, Langmuir 30 (2014) 13970–13978.
[25] A. Lamprou, I. Köse, G. Storti, M. Morbidelli, M. Soos, Synthesis of macroporous polymer particles using reactive gelation under shear, Langmuir 30 (2014) 6946–6953.
[26] B. Brand, M. Morbidelli, M. Soos, Shear-induced reactive gelation, Langmuir 31 (2015) 12727–12735.
[27] M. Bechtle, A. Butte, G. Storti, M. Morbidelli, Preparation of macroporous methacrylate-based monoliths for chromatographic applications by the reactive gelation process, J. Chromatogr. A 1217 (2010) 4675–4681.
[28] A. Lamprou, A.-F.-M. Gavriilidou, G. Storti, M. Soos, M. Morbidelli, Application of polymeric macroporous supports for temperature-responsive chromatography of pharmaceuticals, J. Chromatogr. A 1407 (2015) 90–99.
[29] W. Stöber, A. Fink, E. Bohn, Controlled growth of monodisperse silica spheres in the micron size range, J. Colloid Interface Sci. 26 (1968) 62–69.
[30] V. Tokárová, A. Pittermannová, J. Čech, P. Ulbrich, F. Štěpánek, Thermo-responsive adhesion properties of composite hydrogel microcapsules, Soft Matter 8 (2012) 1087–1095.
[31] K.-S. Chou, C.-C. Chen, The critical conditions for secondary nucleation of silica colloids in a batch Stöber growth process, Ceram. Int. 34 (2008) 1623–1627.
[32] A.S. Siti Shafiqah, Y.M. Amin, R.M. Nor, D.A. Bradley, Effect of particle size on the thermoluminescence (TL) response of silica nanoparticles, Radiat. Phys. Chem. 117 (2015) 102–107.
[33] B. Topuz, D. Şimşek, M. Çiftçioğlu, Preparation of monodisperse silica spheres and determination of their densification behaviour, Ceram. Int. 41 (2015) 43–52.
[34] C.O. Metin, L.W. Lake, C.R. Miranda, Q.P. Nguyen, Stability of Aqueous Silica Nanoparticle Dispersions under Subsurface Conditions.
[35] M.Y. Lin, H.M. Lindsay, D.A. Weitz, R. Klein, R.C. Ball, P. Meakin, Universal diffusion-limited colloid aggregation, J. Phys. Condens. Matter 2 (1990) 3093.
[36] T. Patiño, N. Feiner-Gracia, X. Arqué, A. Miguel-López, A. Jannasch, T. Stumpp, E. Schäffer, L. Albertazzi, S. Sánchez, Influence of Enzyme quantity and distribution on the self-propulsion of non-Janus urease-powered micromotors, J. Am. Chem. Soc. 140 (2018) 7896–7903.
[37] R. Ramesh, P. Puhazhendi, J. Kumar, M.K. Gowthaman, S.F. D'Souza, N.R. Kamini, Potentiometric biosensor for determination of urea in milk using immobilized Arthrobacter creatinolyticus urease, Mater. Sci. Eng. C 49 (2015) 786–792.
[38] C. Sorensen, Light scattering by fractal aggregates: a review, Aerosol Sci. Technol. 35 (2001) 648–687.
[39] C.S. Johnson, Laser Light Scattering, Dover Publication Inc., New York, 1990.
[40] A.S. Moussa, M. Soos, J. Sefcik, M. Morbidelli, Effect of the solid volume fraction on the aggregation and breakage of colloidal suspensions in batch and continuous stirred tank, Langmuir 23 (2007) 1664–1673.
[41] M. Soos, M. Lattuada, J. Sefcik, M. Morbidelli, Interpretation of light scattering and turbidity measurements in aggregated systems: effect of intra-cluster multiple-light scattering, J. Phys. Chem. B 113 (2009) 14962–14970.
[42] L. Ehrl, M. Soos, M. Morbidelli, Dependence of aggregate strength, structure, and light scattering properties on primary particle size under turbulent conditions in stirred tank, Langmuir 24 (2008) 3070–3081.
[43] M. Lattuada, L. Ehrl, Scattering properties of dense clusters of colloidal nanoparticles, J. Phys. Chem. B 113 (2009) 5938–5950.
[44] L. Ehrl, M. Soos, M. Lattuada, Generation and geometrical analysis of dense clusters with variable fractal dimension, J. Phys. Chem. B 113 (2009) 10587–10599.
[45] S. Brunauer, P.H. Emmett, E. Teller, Adsorption of gases in multimolecular layers, J. Am. Chem. Soc. 60 (1938) 309–319.
[46] K. Yoshinaga, T. Yokoyama, Y. Sugawa, H. Karakawa, N. Enomoto, H. Nishida, M. Komatsu, Preparation of monodispersed polymer-modified silica particles by radical polymerization using silica colloid and introduction of functional groups on the composite surface, Polym. Bull. 28 (1992) 663–668.
[47] M. Soos, A.S. Moussa, L. Ehrl, J. Sefcik, H. Wu, M. Morbidelli, Effect of shear rate on aggregate size and morphology investigated under turbulent conditions in stirred tank, J. Colloid Interface Sci. 319 (2008) 577–589.
[48] ANSYS Inc., ANSYS FLUENT 19.2 User's Guide, Canonsburg PA, USA, 2018.
[49] T. Kumaresan, J.B. Joshi, Effect of impeller design on the flow pattern and mixing in stirred tanks, Chem. Eng. J. 115 (2006) 173–193.
[50] P. Meakin, Fractal aggregates, Adv. Colloid Interface Sci. 28 (1988) 249–331.
[51] M. Soos, A. Moussa, L. Ehrl, J. Sefcik, H. Wu, M. Morbidelli, Dynamic response studies of aggregation and breakage dynamics in colloidal dispersions in stirred tanks, J. Dispers. Sci. Technol. 29 (2008) 1–6.
[52] A. Zaccone, M. Soos, M. Lattuada, H. Wu, M.U. Bäbler, M. Morbidelli, Breakup of dense colloidal aggregates under hydrodynamic stresses, Phys. Rev. E 79 (2009), 061401.
[53] M. Soos, L. Ehrl, Mu.U. Bäbler, M. Morbidelli, Aggregate breakup in a contracting nozzle, Langmuir 26 (2009) 10–18.
[54] Y.M. Harshe, M. Lattuada, M. Soos, Experimental and modeling study of breakage and restructuring of open and dense colloidal aggregates, Langmuir 27 (2011) 5739–5752.
[55] D. Saha, M.U. Babler, M. Holzner, M. Soos, B. Luthi, A. Liberzon, W. Kinzelbach, Breakup of finite-size colloidal aggregates in turbulent flow investigated by three-dimensional (3D) particle tracking velocimetry, Langmuir 32 (2016) 55–65.
[56] M. Soos, A. Moussa, L. Ehrl, J. Sefcik, H. Wu, M. Morbidelli, Effect of shear rate on aggregate size and morphology investigated under turbulent conditions in stirred tank, J. Colloid Interface Sci. 319 (2008) 577–589.
[57] L. Ehrl, M. Soos, H. Wu, M. Morbidelli, Effect of flow field heterogeneity in coagulators on aggregate size and structure, AIChE J. 56 (2010) 2573–2587.
[58] M. Lin, H. Lindsay, D. Weitz, R. Ball, R. Klein, P. Meakin, Universal reaction-limited colloid aggregation, Phys. Rev. A 41 (1990) 2005.
[59] M. Kerker, The Scattering of Light, Academic Press, New York, 1969.
[60] A.R. Jones, Lights scattering for particle characterization, Prog. Energy Combust. Sci. 25 (1999) 1–53.
[61] I.M. Šapić, L. Bistričić, V. Volovšek, V. Dananić, Vibrational analysis of 3-glycidoxypropyltrimethoxysilane polymer, Macromol. Symp. 339 (2014) 122–129.
[62] P.S. Chaudhari, A. Gokarna, M. Kulkarni, M.S. Karve, S.V. Bhoraskar, Porous silicon as an entrapping matrix for the immobilization of urease, Sens. Actuators B Chem. 107 (2005) 258–263.